J Mammal Evol
https://doi.org/10.1007/s10914-017-9416-7

ORIGINAL PAPER

Virtual Endocast Morphology of Mesotheriidae (Mammalia, Notoungulata, Typotheria): New Insights and Implications on Notoungulate Encephalization and Brain Evolution

Marcos Fernández-Monescillo[1] · Pierre-Olivier Antoine[2] · François Pujos[1] · Helder Gomes Rodrigues[3,4] · Bernardino Mamani Quispe[5] · Maeva Orliac[2]

Abstract We provide morphological, quantitative, and qualitative studies of cranial endocasts of mesotheriid notoungulates solving previous open debate on notoungulate endocasts. For that purpose, we use the most accurate digital reconstructions methods. We confirm that mesotheriids have endocasts similar in shape and gyrification to those of other rodent-like notoungulates (i.e., Hegetotheriidae and Interatheriidae) and living cavy rodents (e.g., *Dolicavia minuscula*, *Hydrochoerus*, and *Cavia*). We identify these similarities as evolutionary response to potentially similar ecological constraints. Based on the encephalization quotient (EQ) of several notoungulate families (i.e., Mesotheriidae, Interatheriidae, Notohippidae, Toxodontiidae, and Hegetotheriidae), there seems to be no increase in terms of EQ or neocortical complexity through time in that group. In addition, comparison with several Holarctic 'euungulates' leads us to propose differential predation pressure as a potential driver for EQ. Among notoungulates, braincase comparison between well-known Oligocene–Pleistocene mesotheriids and other families identifies lifestyle as an additional possible driver for EQ, with lower values for semifossorial taxa, in a similar way to rodents. Finally, the observed stability of mesotheriid EQ (from the Oligocene to the Pliocene) would match a conservative lifestyle further reflected by their highly invariant appendicular skeleton.

Keywords South America · Bolivian Altiplano · Paleomammalogy · Paleoneurology · Computed tomography (CT) · Digital cranial endocast · Ungulate brains · Stasis

Electronic supplementary material The online version of this article (https://doi.org/10.1007/s10914-017-9416-7) contains supplementary material, which is available to authorized users.

✉ Marcos Fernández-Monescillo
mfernandezmonescillo@gmail.com

[1] Instituto Argentino de Nivología Glaciología y Ciencias Ambientales (IANIGLA), CCT–CONICET–Mendoza, Avda. Ruiz Leal s/n, Parque Gral. San Martín, 5500 Mendoza, Argentina

[2] Institut des Sciences de l'Evolution, cc64, Université de Montpellier, CNRS, IRD, EPHE, F-34095 Montpellier, France

[3] Department of Origines et évolutions, Sorbonne Universités, CR2P, UMR CNRS 7207, Université de Paris 06, Muséum national d'Histoire naturelle, 8 rue Buffon, 75005 Paris, France

[4] Mécanismes adaptatifs et évolution (MECADEV), UMR 7179, CNRS, Funevol team, Muséum National d'Histoire Naturelle, 55 rue Buffon, Bat. Anatomie Comparée, CP 55, 75005 Paris Cedex 5, France

[5] Departamento de Paleontología, Museo Nacional de Historia Natural, Calle 26 s/n, Cota Cota, La Paz, Bolivia

Introduction

The Order Notoungulata includes 13 families of South American native ungulates. As such, it is considered as one of the most successful and most diversified endemic South American clades throughout the Cenozoic (Simpson 1948; Cifelli 1985, 1993; Marshall and Cifelli 1989; McKenna and Bell 1997; Croft 1999). The two traditionally recognized suborders, Toxodontia and Typotheria, are commonly considered as being monophyletic (Billet 2011). Typotheria were primarily typified by "*Typotherium,*" today assigned to *Mesotherium.* Typotheria include small to medium-sized notoungulates (Patterson and Pascual 1968; Bond 1986; Croft et al. 2004; Billet et al. 2008; Elissamburu 2012). Mesotheriidae, which belong to Typotheria, are also monophyletic. They include

the late Oligocene Trachytheriinae (a paraphyletic group typified by the genus *Trachytherus*) and the monophyletic Miocene–early Pleistocene Mesotheriinae (Billet 2011).

Serres (1867) described the endocast of the mesotheriid *Mesotherium* sp., which corresponds to the first endocast description for a South American native ungulate, later figured and analyzed in details by Gervais (1872). Thereafter, other natural mesotheriid endocasts have been described for *Trachytherus spegazzinianus* (Loomis 1914; Patterson 1934), *Typotheriopsis internum* (Patterson 1937; Radinsky 1981), *Mesotherium* sp. (Dechaseaux 1962), and *Pseudotypotypotherium pseudopachygnatum* (Radinsky 1981). Computed tomography (i.e., CT scan) now offers an unprecedented opportunity to gain access to detailed reconstructions of internal cranial cavities, essential for endocast studies. Previous notoungulates and litoptern endocast studies (Radinsky 1981; Dozo and Martínez 2015; see Online Resource 1) mainly focused on neuromorphological aspects (e.g., neocortical expansion, gyrification pattern, relative frontal lobe size), and relative brain size (i.e., encephalic volume [EV], body mass estimates [BM], and neocortex expansion; Radinsky 1981; see Online Resource 2).

The phylogenetic position of notoungulates within extant placental mammals has been debated through the last centuries (Serres 1867; Gregory 1910; McKenna 1975). Recent proteomic-based phylogenetic studies based on proteomic data locate the notoungulate *Toxodon* sp. and the litoptern *Macrauchenia* sp. as sister taxa within the Panperissodactyla, i.e., closer to Perissodactyla than to any other extant placental orders (Buckley 2015; Welker et al. 2015). It is important to know the phylogenetic affinities with extant animals, in order to study and compare properly the modification of the fossil taxa, within a temporal framework, especially in the case of the notoungulates, which have no living representatives. The aims of the present work are to: (i) describe for the first time in detail the endocast morphology of the mesotheriids *Trachytherus alloxus* (late Oligocene, Deseadan SALMA), *Eutypotherium superans* (middle Miocene), *Plesiotypotherium achirense* and *Mesotherium maendrum* (early Pliocene Montehermosan SALMA); (ii) compare the new data obtained with previously described cranial endocasts of *T. spegazzinianus* (Loomis 1914; Patterson 1934) and *Mesotherium* sp. (Serres 1867; Gervais 1869, 1872; Dechaseaux 1962), and eventually complete further the concerned descriptions; (iii) estimate the encephalization quotient (EQ), the neocortical ratio (NR), and the piriform ratio (PR) of Mesotheriidae; and (iv) analyze the relative size of the brain and the circumvolution patterns of mesotheriids in comparison to other Notoungulata and Holarctic placentals (living and extinct). Finally, we provide a possible paleoecological explanation of the paleoneurological differences observed within mesotheriids, based on lifestyle, behavior, and predatory pressure differentiations in notoungulates.

Material

Institutional Abbreviations

AMNH, American Museum of Natural History, New York, USA; CNP-ME, endocast collection, Centro Nacional Patagónico, Puerto Madryn, Chubut, Argentina; FMNH Radinsky collection of the Department of Geology, Field Museum of Natural History, Chicago, USA; IANIGLA-PV, Instituto Argentino de Nivología, Glaciología y Ciencias Ambientales, Vertebrate Paleontology, Mendoza, Argentina; MACN, Museo Argentino de Ciencias Naturales, Buenos Aires, Argentina: specimens referred to in the text as "Pv" (National Collections of Paleovertebrates) or "A" (Ameghino collection), respectively; MCZ, Museum of Comparative Zoology, Harvard University, Cambridge, USA; MMP, Museo Municipal de Ciencias Naturales de Mar del Plata, Argentina; MNHN, Muséum national d'Histoire naturelle, Paris, France; MNHN-Bol, Museo Nacional de Historia Natural de Bolivia, La Paz, Estado Plurinacional de Bolivia; MPEF-PV, Museo Paleontológico Egidio Feruglio, Paleontología Vertebrados, Trelew, Chubut, Argentina; UCMP, University of California Museum of Paleontology, Berkeley, USA; UNPSJB-PV, Repositorio Científico y Didáctico de la Facultad de Ciencias Naturales de la Universidad Nacional de La Patagonia San Juan Bosco, Comodoro Rivadavia, Chubut, Argentina.

Trachytheriine Mesotheriid Specimens

Trachytheriinae are represented by a natural cranial endocast of the Oligocene species *T. spegazzinianus* (UNPSJB PV-112, Fig. 1a–d) from Cabeza Blanca (Argentina, Deseadan SALMA; see Billet et al. 2008 for further details). This specimen documents a complete endocast, contrary to what is mentioned in the description provided by Patterson (1934). We also describe the digital reconstruction of a subadult incomplete specimen of *T. alloxus* (MNHN Bol V 6335, holotype) from Salla (Bolivia, Deseadan SALMA), preserving the olfactory bulbs and the neocortical gyrification.

Mesotheriine Mesotheriid Specimens

Our study includes the digital endocast of: (i) one specimen of *E. superans* (MACN A 11079, holotype; Kraglievich 1930) with broken olfactory bulbs, ventral brain stem, and poorly preserved neocortex surface; (ii) three specimens of *P. achirense* including one subadult (MNHN-Bol-V 12664), with the dorsal surface of the endocast neocortex, and two adults: MNHN.F.ACH 26 (holotype; Fig. 2a–c) with remarkably preserved neocortical surface and MNHN-Bol-V 8507, dorsoventrally flattened and with a dorsal neocortex badly preserved. All the specimens collected in Achiri are housed

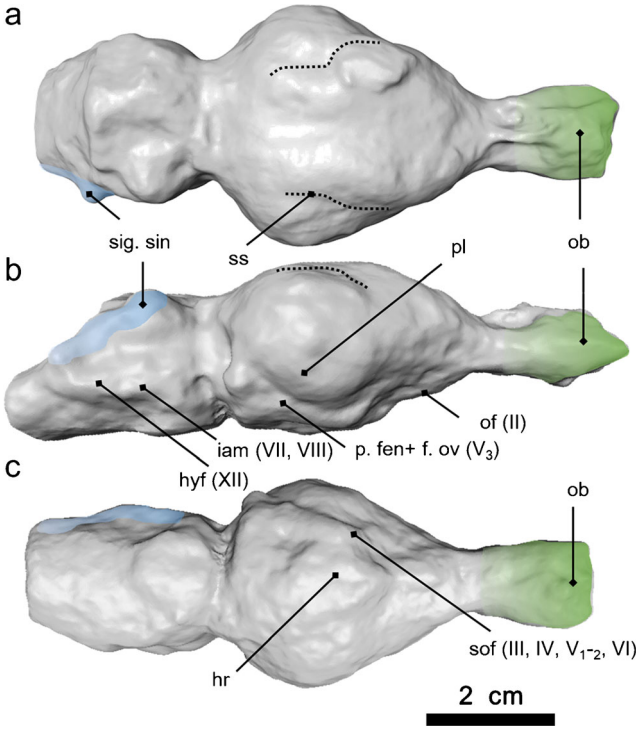

Fig. 1 Digital cranial endocast of *Trachytherus spegazzinianus* (UNPSJB PV-112). **a**, dorsal view; **b**, right lateral view; and **c**, ventral view. Abbreviations: *hr* hypophyseal region, *hyf* cast of hypoglossal foramen (exit of cranial nerve XII), *iam* cast of internal auditory meatus (exit of cranial nerves VII,VIII), *ob* olfactory bulbs, *of* cast of optic foramen (exit of cranial nerve II), *p. fen + f. ov* (V_3) piriform fenestra + foramen ovale (exit of cranial nerve V_3), *pl* piriform lobe, *sc* suprasylvian convolution, *sig. sin* sigmoid sinus, *sof* cast of sphenorbital fissure (exit of cranial nerves III, IV, V_1 and V_2, VI), *ss* sylvian or suprasylvian sulcus

in the MNHN-Bol, La Paz, Bolivia and in the MNHN, Paris, France; (iii) two specimens of *M. maendrum,* MACN Pv 2925 (Fig. 3a–c) complete and well preserved, and MACN Pv 1111 well preserved except for the olfactory bulbs (Montehermosan; Rovereto 1914; Cattoi 1943); and (iv) one specimen of *M. cristatum* (holotype MNHN.F.PAM 2; Fig. 4a–c) with the right half of the endocast (late early Pleistocene Ensenadan SALMA; Serres 1867).

Specimens for Comparison

Regarding South American mammals, our comparative material consists of cranial endocasts of non-mesotheriid Typotheria and of Toxodontia among Notoungulata, and of a litoptern (see Online Resource 1). A comparison is made with several living and extinct artiodactyl endocasts (Orliac and Gilissen 2012), for they share similar dietary preferences, under very distinct predation pressures (Croft 2001). Finally, comparisons are made with some rodent endocasts (Bertrand et al. 2016), because of similarities between notoungulates and rodent endocasts as highlighted in mesotheriids (Radinsky 1984; Dozo 1997) and in other rodent-like notoungulates (e.g., Patterson 1934; Reguero and Prevosti 2010).

Methods

CT-Scan Procedure and Parameters

The skulls of *P. achirense* (MNHN.F.ACH 26) and of *M. cristatum* (MNHN.F. PAM 2) were scanned at the MNHN using the AST-RX facility (ca. 450 endocast slices, resolution 6.7843 length. And 4.9480 width pixels; with a voxel size of 73.7 μm after scaling 147.7 μm, and 101.1 μm after scaling 202.1 μm, respectively). Other skulls of *P. achirense* (MNHN-Bol-V 8507, 12,664) and *T. alloxus* (MNHN-Bol-V 6355) were scanned at the Clínica MEDICENTRO of La Paz (Estado Plurinacional de Bolivia) using a Philips MX 8000 clinical CT scanner (ca. 200 slices at 140 kV and 300 mA; 0.26 mm pixel size and 0.75 mm interslice). The skull of *M. maendrum* (MACN Pv 2925) was scanned at the Fundación Escuela Medicina Nuclear (FUESMEN) of Mendoza, Argentina, using a General Electric Lightspeed 16 clinical CT scanner (at 140 kV and 200 mA). Finally, the skulls of *M. maendrum* (MACN Pv 1111) and *E. superans* (MACN A 11079) were scanned at the Fundación de Diagnóstico Nuclear (FCDN) of Buenos Aires, Argentina, using General Electric Lightspeed clinical CT scanner (at 140 kV and 200 mA). We extracted the digital endocast of the braincase using the segmentation tools of AVIZO 10.0 (FEI Visualization Sciences Group). Because of the presence of sediment and recrystallization in the braincase space, the segmentation process was carried out slice-by-slice manually with the density delimited range on the brush tool of AVIZO 10.0 to discern bone form sediment, and thus generate the surface using unconstrained smoothing with a value of ca. 3.5–4.

Photogrammetry

The surface of the natural cranial endocast of *T. spegazzinianus* (UNPSJB PV-112) included in the study and associated cranial elements were modelled in 3D and scaled using photogrammetry with Agisoft PhotoScan (Agisoft LLC 2010, www.agisoft.com).

Linear Measurements, Body Size, Endocast Volume, and Neocortical Surface Estimate

The endocast measurements (see Online Resource 3) were taken following Macrini (2009) and endocast flexure angle estimates (Table 1) were measured according to Macrini et al. (2007). Linear measurements and volumes were taken using Netfabb (basic version, Autodesk 2016; see Tables 1

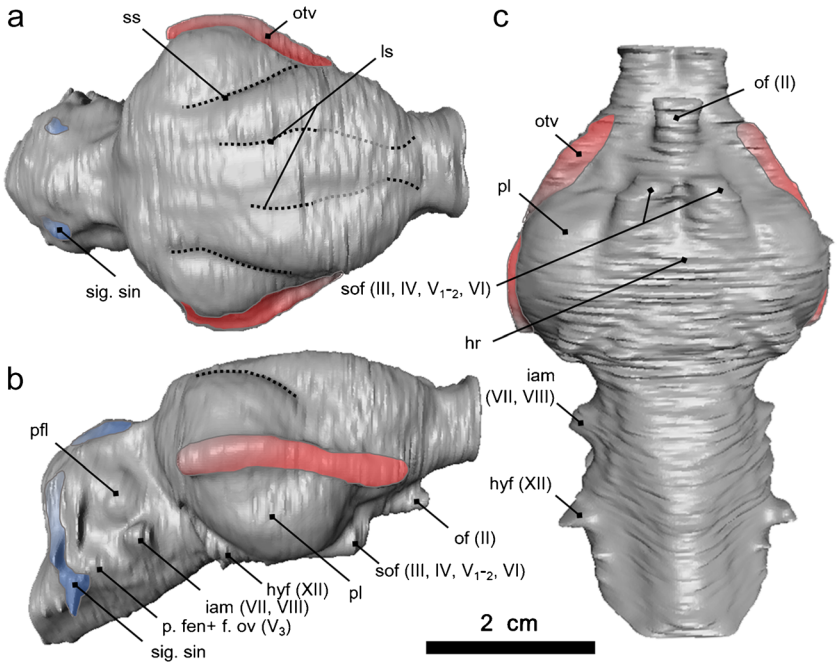

Fig. 2 Digital cranial endocast of *Plesiotypotherium achirense* (MNHN.F.ACH 26, holotype). **a**, dorsal view; **b**, right lateral view; and **c**, ventral view. Abbreviations *hr* hypophyseal region, *hyf* cast of hypoglossal foramen (exit of cranial nerve XII), *iam* cast of internal auditory meatus (exit of cranial nerves VII,VIII), *lc* lateral convolution, *ls* lateral sulcus, *ob* olfactory bulbs, *of* cast of optic foramen (exit of cranial nerve II), *op* olfactory peduncles, *otv* orbitotemporal vessel, *p. fen + f. ov* (V_3) piriform fenestra + foramen ovale (exit of cranial nerve V_3), *pfl* paraflocculus, *pl* piriform lobe, *sig. sin* sigmoid sinus, *sof* cast of sphenorbital fissure (exit of cranial nerves III, IV, V_1 and V_2, VI), *ss* sylvian or suprasylvian sulcus

and 2). Finally, we used ISE-MeshTools (version 1.3.3; Lebrun 2014; Lebrun and Orliac 2017) to estimate the surface of the neocortex and the total surface of the endocast and olfactory bulbs (Table 2, Online Resource 3), and to compare with other mesotheriids through time (Online Resource 2).

The body mass (BM) estimates of fossil taxa having no extant representatives, such as notoungulates and litopterns, are generally controversial because of the absence of feedback control and in some cases the extreme variation between lower and high estimated values (Croft et al. 2004; Elissamburu

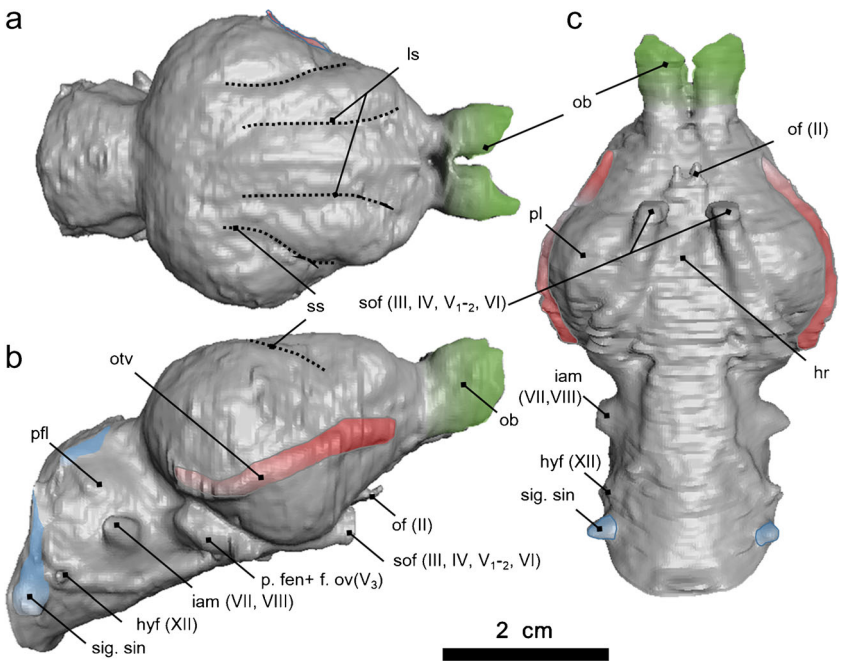

Fig. 3 Digital cranial endocast of *Mesotherium maendrum* (MACN Pv 2925). **a**, dorsal view; **b**, right lateral view; and **c**, ventral. Abbreviations: *hr* hypophyseal region, *hyf* cast of hypoglossal foramen (exit of cranial nerve XII), *iam* cast of internal auditory meatus (exit of cranial nerves VII,VIII), *ls* lateral sulcus, *ob* olfactory bulbs, *of* cast of optic foramen (exit of cranial nerve II), *otv* orbitotemporal vessel, *p. fen + f. ov* (V_3) piriform fenestra + foramen ovale (exit of cranial nerve V_3), *pfl* paraflocculus, *pl* piriform lobe, *sig. sin* sigmoid sinus, *sof* cast of sphenorbital fissure (exit of cranial nerves III, IV, V_1 and V_2, VI), *ss* sylvian or suprasylvian sulcus

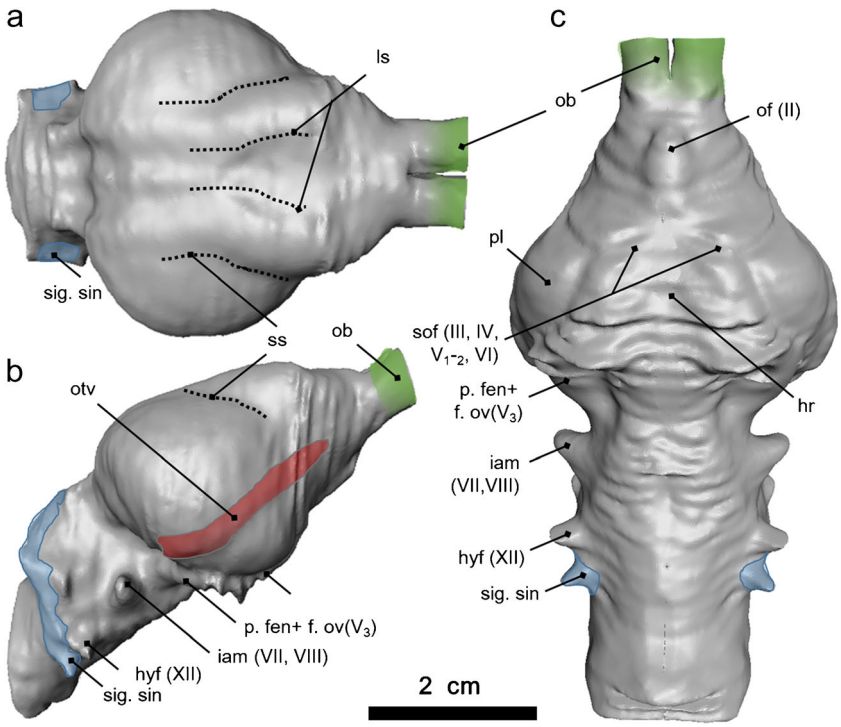

Fig. 4 Digital cranial endocast of *Mesotherium cristatum* (MNHN.F.PAM2, holotype). **a**, dorsal view; **b**, ventral view; **c**, right lateral view; and **d**, left lateral view. Abbreviations: *hr* hypophyseal region, *hyf* cast of hypoglossal foramen (exit of cranial nerve XII), *iam* cast of internal auditory meatus (exit of cranial nerves VII,VIII), *ls* lateral sulcus, *ob* olfactory bulbs, *of* cast of optic foramen (exit of cranial nerve II), *otv* orbitotemporal vessel, *p. fen + f. ov* (V_3) piriform fenestra + foramen ovale (exit of cranial nerve V_3), *pl* piriform lobe, *sig. sin* sigmoid sinus, *sof* cast of sphenorbital fissure (exit of cranial nerves III, IV, V_1 and V_2, VI), *ss* sylvian or suprasylvian sulcus

2012; see Online Resource 2). We estimated the EQ using several BM methods to test how the BM affects EQ. The previous methods used vary between univariates (e.g., Scott 1990; Janis 1990; Croft 2000, 2016; Croft et al. 2004) to multivariate methods (i.e., Mendoza et al. 2006), and others (e.g., 3D landmarks; Cassini et al. 2012a, b). We also used a similar method to that of Elissamburu (2012) based on an exhaustive bibliographical revision of BM. We have proceeded as follows: (i) we revised and completed previous BM reviews (e.g., Elissamburu 2012) to create an updated bibliographical review of BM of the taxa included in this study and dismissed the values we considered under- or overestimated and calculated the mean value (for all taxa we considered at the species level, except for mesotheriids for which we used each specimen) (see Online Resource 2); (ii) in order to be accurate, we have used for the original new taxa described, the "algorithm 4.1" defined by Mendoza et al. (2006; Online Resource 2), which specifically focused on extinct ungulates: BM = 0,736 SUML +0,606 SUMW +0,530 MZW + 0,621 PAW +0,741 SC – 0,157 SD + 0,603 (based on craniodental measurement; Online Resource 2, 3); and, finally, (iii) we have also estimated the BM without dismissing any value (Online Resource 2) in order to check how overestimated values affect calculated EQs.

We have used the two commonly used EQ equations: EQ1 (EQ1 = EV/0.12 (EM) $^{0.67}$, with EM = estimated body mass, defined by Jerison 1973), or EQ2 (EQ2 = EV/0.055 (EM) $^{0.74}$, defined by Eisenberg 1981) (Table 2; Online Resource 2). We have tested statistically the artiodactyls/notoungulates EQ differences for Oligocene and Miocene taxa, using the Student t test of the statistic software package IBM SPSS Statistic. 19.0 (Online Resource 4).

We have compared these new EQ estimates of Oligocene-Pleistocene notoungulates and litopterns with previous EQ estimates (using previous encephalic volume data from the literature; see Online Resource 2), with that of the best-represented family (i.e., Mesotheriidae). We have then examined factors that could be responsible for the observed differences in terms of lifestyle and behavior, at the scale of Holarctic ungulates, by comparing predatory pressure (e.g., Holarctic ungulates were exposed to large carnivorous mammals, while notoungulates were exposed to non-mammalian 'small brained' predators (Jerison 1973; Croft 2001). In order to analyze more exhaustively the endocast of the mesotheriids, we have calculated the neocorticalization ratio (NR; Jerison 2012). The NR corresponds to the surface area of neocortex relative to the entire endocast surface area reduced by olfactory bulbs (Jerison 2012): NR = total neocortex surface area/ (total surface area – olfactory bulbs surface area). Finally, to discuss the olfactory sense of mesotheriids: (i) we have introduced and calculated for the first time the piriform ratio (PR) as the piriform cortex surface in relation to the endocast surface area: PR = total piriform lobes surface/ total surface area-olfactory bulbs surface area; (ii) we have measured the olfactory peduncles area (peduncles height [OPH] *peduncles width [OPW]); Table 1), which gives an idea of the total olfactory fibers that cross the olfactory bulbs and of the surface area of the olfactory bulbs (OB) (only preserved in *T. spegazzinianus* and *M. maendrum*).

Table 1 Digital endocast linear measurements in millimeters (see Online Resource 3). Endocast linear measurements adapted from Macrini (2009) and Dozo and Martínez (2015)

Specimen number ➔	UNSJPV 112	MACN A 11079 (holotype)	MNHN-Bol-V 12664	MNHN.F. ACH26 (holotype)	MNHN-Bol-V 8507	MACN Pv 2925	MACN Pv 1111	MNHN.F.PAM 2 (holotype)
Species➔	*Trachytherus spegazzinianus*	*Eutypotherium superans*	*Plesiotypotherium achirense*	*Plesiotypotherium achirense*	*Plesiotypotherium achirense*	*Mesotherium maendrum*	*Mesotherium maendrum*	*Mesotherium cristatum*
EL	102.15		71.21	81.86	*68.03*	85.71	68.41	72.19
EL-OB	75.51	63.24	61.52	79.84	64.7	70.1	62.03	62.5
CRL	48.84	42.43	40.78	51.42	44.96	51.14	49.67	43.67
CRW	47.08	40.75	39.24	50.07	43.3	56.68	48.74	46.9
FRW	28.01	28.01	25.35	30.92	30.02	35.25	29.75	22.77
CRH	31.16		29.57	34.07	29.97	39.84	32.7	29.45
OBL	25.72		*10.72*	7.58		15.82	*10.09*	12.93
OBW	18.76		15.32	18.75	15.66	20.73	17.8	15.11
OPW[a]	15.16	11.66	12.78	15.68	15.82	17.99	14.71	13.81
OPH[a]	8.42	9.27	11.23	13.64	8.55	14.82	13.19	8.63
OBH	15.21		13	13.23	*7.9*	16.06	12.96	12.02
PLD	29.58	30.94	23.34	28.23	27.75	30.02	26.23	29.72
CBL	24.58		18.09	23.49	19.24	17.3	13.44	19.16
CBW	31.45		21.85	28.86	25.29	32.55	28.67	24.37
HBH	29.81			39.73	31.77	40.34	46.81	31.6
HPL	15.89	5.45	*10.12*	10.87			8.7	6.94
HPW	9.44	6.1	6.76	18.75		12.16	6.41	7.99
OPWxOPH[a]	127.65	108.09	143.52	213.88	135.26	266.61	194.02	119.18
FRW/CRW Ratio	1.68	1.45	1.55	1.62	1.44	1.61	1.64	2.06
OBW/FRW Ratio	1.49		1.65	1.65	1.98	1.70	1.67	1.51
EL-OB/CBL Ratio	0.33		0.29	0.29	0.30	0.25	0.22	0.31
Flexure angle	20.01		24.7	30.45		32.28	27.93	31.14

Abbreviations: CBL maximum length of cerebellar cast, *CBW* maximum width of cerebellar cast, *CRH* maximum height of cerebral cast, *CRL* maximum length of cerebral cast exclusive of olfactory bulbs, *CRW* maximum width of cerebral cast, *EL* maximum length of endocast, *EL-OB* maximum length of endocast exclusive of olfactory bulbs, *FRW* maximum width of frontal region, *HBH* maximum height of hindbrain cast, *HPL* maximum length of hypophysis cast, *HPW* maximum transverse width of hypophysis cast, *OBH* maximum height of olfactory bulb casts, *OBL* maximum length of olfactory bulb casts, *OBW* maximum combined width of olfactory bulb casts, *OPW* olfactory peduncles width, *PLD* maximum distance between ventral edges of piriform lobes. In italic appear estimated or approximate measurements, volumes or surfaces

[a] Not appear in the linear measurements or ratios from Macrini (2009) nor Dozo and Martinez (2015)

Table 2 Data for relative brain size, neocortical ratios (NR) and surface of the neocortex for the mesotheriids compared

Species	Number	EV (cm^3)	BM[a] (kg)	EQ1 (Jerison 1973)	EQ2 (Eisenberg 1981)	Total endocast surface (mm^2)	Total endocast surface (no OB) (mm^2)	Total volume OB (cm^3) (percentage of the total volume)	Neocortex surface (mm^2)	Neocortical ratio (no OB)	Piriform surface (mm^2)	Piriform ratio (no OB)
Trachytherus spegazzinianus	UNSJPV 112	60.41	136.46	0.19	0.17	10,441	9288	2.96 (4.89%)	2860	30.79%	467.38	5.03%
Trachytherus alloxus	MNHN-Bol-V 6355(holotype)	30.89	45.28	0.20	0.13	6062						
Eutypotherium superans	MACN A 11079 (holotype)	47.36	71.90	0.23	0.22		*8944*				424.68	*4.75%*
Typotheriopsis "*insigne*"	FMNHN 14477	85	125.28	0.28	0.26							
Plesiotypotherium achirense	MNHN-Bol-V 12664	*30.46*	52.74	0.18	0.18				1948.4		463.48	
Plesiotypotherium achirense	MNHN-Bol-V 8507	38.72	69.88	0.19	0.18		8703		2254.8	25.90%	409.26	4.70%
Plesiotypotherium achirense	MNHN.F.ACH 26 (holotype)	72.42	76.18	0.33	0.32		11,136		2334	20.95%	719.38	6.45%
Mesotherium maendrum	MACN Pv 1111	65.34	154.06	0.19	0.17		9777		2939.8	30.06%	585.26	5.98%
Mesotherium maendrum	MACN Pv 2925	93.25	194.82	0.23	0.21	13,608	12,641	2.81 (2.99%)	4133.4	32.69%	788.86	6.24%
Mesotherium cristatum	MNHN.F.PAM 2 (holotype)	54.23	196.28	0.13	0.12		9319		2210	23.71%	360.12	3.86%

In italics appear estimated and approximate measurements, volumes or surfaces

Abbreviations: BM body mass, *EQ* encephalization quotient, *EV* encephalic volume, *OB* olfactory bulbs

[a] BM method (see Online Resource 2)

Anatomical Description

We follow the terminology used by Dozo and Martínez (2015) based on Simpson (1932, 1933a, b), Patterson (1937), Brauer and Shober (1970), Radinsky (1978, 1981), Dozo (1997), and Macrini (2009). In addition, a different nomenclature of sulci in extant rodents (Campos and Welker 1976) is used here in the comparison section.

All data generated or analyzed during this study are included in this published article [and its supplementary information files].

Results

Description and Comparison

We describe here mesotheriid endocasts following distinct brain sections (i.e., rhinencephalon, neopallium, midbrain, and cerebellum). Some morphological aspects were not discussed in previous studies by Radinsky (1981) or Dozo and Martínez (2015). Comparisons with previously described or figured notoungulate endocasts are available in Online Resource 1.

Rhinencephalon

In most cases, the olfactory bulbs are not perfectly preserved due to the breakage of the cribriform plate (except for *T. spegazzinianus* and *M. maendrum,* MACN Pv 2925). In most taxa, the olfactory bulbs (OB) are separated in the sagittal plane. The olfactory peduncles are short and not covered by the rostral extension of the neocortex. The olfactory bulbs of *T. spegazzinianus* (UNSPJV 112) are proportionally more elongated and exclusively rostrally oriented than those, rostrodorsally oriented, of *M. maendrum* (MACN Pv 2925). In lateral view (Fig. 1c, d), the OB also points more dorsally in *T. alloxus* and mesotheriines than in *T. spegazzinianus* (Figs. 2c–d, 3c–d and 4c–d); the rhinal fissure is not observed in *T. spegazzinianus*. The volume of the piriform lobe in comparison to the total endocast surface is similar for *T. spegazzinianus* (ca. 5%) and other mesotheriine specimens (with values ca. 4–6%; Table 2 and Fig. 5), among which *P. achirense* (MNHN.F. ACH 26) and *M. maendrum* (MACN Pv 2925) show the highest values of the piriform cortex; surprisingly the derived species *M. cristatum* shows the lowest values (3.86%). The maximum width of the endocast is located at the level of the lateral borders of the neopallium. A similar rostral location of the rhinal fissure is observed in other notoungulates, such as the hegetotheriid typothere *Hegetotherium mirabile*, but also the notostylopid *Notostylops* sp. (Simpson 1933a), and the Toxodontia *Rhyphodon* sp. (isotemniid) (Simpson 1933b; Dozo and Martínez 2015, *Rhynchippus equinus* (notohippid) (Patterson 1937; Dozo and Martínez 2015 Radinsky 1981), and *Adinotherium* sp. (toxodontid) (Radinsky 1981; Dozo and Martínez 2015). Olfactory bulbs are bifurcated in most notoungulates, but a morphotype similar to that of *T. spegazzinianus* is found in the interatheriids *Miocochilius anomopodus* (Stirton 1953), while the other morphotype would be similar to that of the *Protypotherium* sp. (interatheriid) (Simpson 1933b; Dechaseaux 1962; Dozo and Martínez 2015).

The olfactory bulbs are well preserved in *T. spegazzinianus* (UNSPJV 112) and *M. maendrum* (MACN Pv 2925). Their volume equals ca. 5% and ca. 3% of the total endocast volume, respectively (Table 2). For other taxa, the rostral part of the olfactory bulbs is not preserved, so we have used the maximum width of the uncompletely preserved olfactory bulbs, and the area of the olfactory peduncles (height of the olfactory peduncles (OPH) * width (OPW) to provide a general idea of the number of olfactory fibers (Table 1). The area of the olfactory peduncles is higher in *M. maendrum* (MACN Pv 2925) and in *P. achirense* (MNHN.F.ACH 26) followed by *T. spegazzinianus* and finally *E. superans* and *M. cristatum* show the lowest values (Table 1).

Neopallium

The rhinal fissure is considered as the external identifier of the limit between the neocortex and paleocortex (Jerison 1973; Long et al. 2015). It is visible rostrally in mesotheriines and probably hidden caudally by the orbitotemporal canal, which is sometimes considered as the exterior hallmark of the rhinal fissure location (e.g., Rowe 1996; Silcox et al. 2011). However, in the litoptern *Huayqueriana* cf. *H. cristata* (Forasiepi et al. 2016), and in the toxodontids *Rhynchippus equinus* (Dozo and Martínez, 2015), and *Toxodon* sp. (Dechaseaux 1962), both the rhinal fissure and the orbitotemporal canal have distinct courses, which questions the validity of considering the orbitotemporal canal as a marker of the rhinal fissure location.

The rhinal fissure of notoungulates shows the same transversal (rostrocaudal) position over the piriform lobe; in most taxa, it appears only in the rostral most part of the neocortex (e.g., the notostylopid *Notostylops,* the notohippids *Eurygenium latirostris* and *Rhynchippus equinus*, and the toxodontid *Toxodon* sp.), while in others (e.g., the interatheriid typothere *Miocochilius anomopodus*), it runs all along the endocast. Macrini (2006) indicated that the rhinal fissure is not always visible on the endocast, as is the case for the specimen of the trachytheriine *T. spegazzinianus*, in which neither the rhinal fissure nor the orbitotemporal canal are visible (as in Patterson 1934) (Fig. 1b). In *T. alloxus*, the orbitotemporal fissure seems to be laterally and rostrodorsally oriented (Online Resource 4), and therefore we infer the rhinal fissure

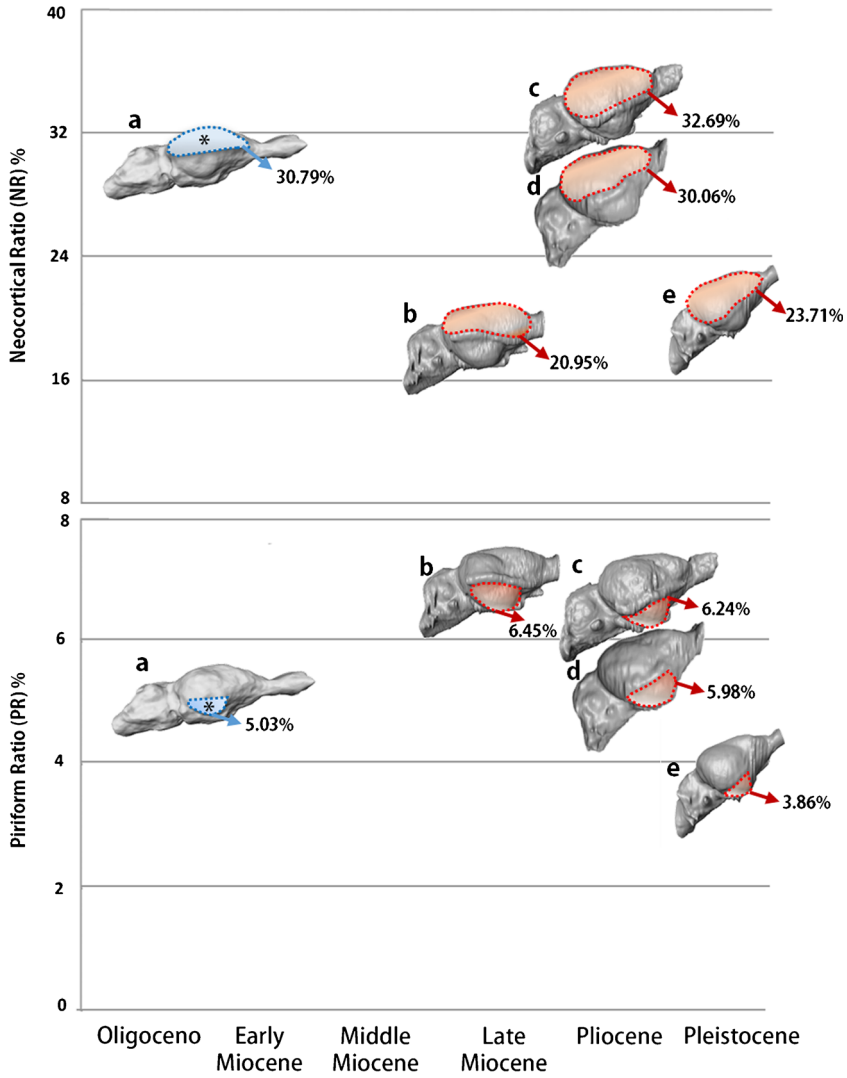

Fig. 5 Estimate of the neocorticalization ratio (NR) and the piriform ratio (PR) surfaces through time (percentages). Trachytheriines (Oligocene, blue and marked with *) and mesotheriines (early Miocene-Pleistocene, red). **a**, *Trachytherus spegazzinianus* (UNSJPV 112). **b**, *Plesiotypotheirum achirense* (MNHN.F.ACH 26, holotype). **c, d**, *Mesotherium maendrum* (MACN Pv 2925 and MACN Pv 1111). **e**, *Mesotherium cristatum* (MNHN.F.PAM 2, holotype)

has the same location as in other mesotheriid endocasts previously described.

The gyrification of the neocortex in *T. spegazzinianus* only consists of a shallow suprasylvian sulcus (Fig. 1a). However, in *T. alloxus* and in the mesotheriines *P. achirense, M. maendrum*, and *M. cristatum*, the neocortex shows a more complex pattern of sulci (Figs. 2a, 3a, 4a, and Online Resource 4). In addition to a marked suprasylvian sulcus, *T. alloxus* shows a lateral sulcus in the caudal portion of its endocast, close to the sagittal plane. All three specimens of *P. achirense* studied here present slight variations in their sulci pattern, especially in the length of the suprasylvian sulcus (Figs. 2a; Online Resource 4). Indeed, in the subadult specimen MNHN-Bol V 12664, the suprasylvian sulcus is elongated and the lateral sulcus is moderately long and rostrally divergent. The specimen MNHN-Bol V 8507 is poorly preserved and only a short suprasylvian sulcus is present. Finally, the specimen MNHN.F.ACH 26 shows a well-developed sylvian sulcus, medially a short lateral sulcus, and rostrally a short coronal sulcus. The two studied specimens of *M. maendrum* also show variation in their sulci pattern (Fig. 3a; Online Resource 4): MACN Pv 2925 bears a long suprasylvian sulcus and an extended lateral sulcus that diverge rostrally from the parasagittal plane. MNHN Pv 1111 shows a long suprasylvian sulcus, a short transversal sulcus (divergent from the latter), and rostrally, probably the rostralmost extension of the lateral sulcus, absent caudally. The holotype of *M. cristatum* (MNHN.F.PAM 2) exhibits a marked suprasylvian sulcus and, in the caudal part of the cerebrum, a short and rostrally convergent sulcus. In addition to the latter sulci, and parallel and medial to the suprasylvian sulcus, lies a deep and short lateral sulcus (Fig. 4a). A similar gyrification pattern is observed in the endocast of *Mesotherium* sp. described by Dechaseaux (1962). A suprasylvian sulcus rostrally divergent is recognized in all the notoungulates compared, except in *Rhyphodon*, which appears laterally concave. The suprasylvian sulcus is the only sulcus observed in the toxodonts *Rhyphodon* sp. and *Leontinia* sp., and in the early

mesotheriid *T. spegazzinianus*. Other notoungulates show a more complex gyrification pattern, with the presence of at least a lateral sulcus medially located, as in *T. alloxus* and mesotheriines. In addition to the suprasylvian and lateral sulci, toxodonts show in general a much more complex gyrification: the giant homalodotheriid *Homalodotherium cunninghami* shows a shorter and rostrally divergent pair of sulci in the caudal border of the cerebrum (Patterson 1937); the notohippid *Rhynchippus equinus* shows a short and transversal ectosylvian sulcus located laterally to the ectosylvian convolution and, in the rostral part, a short additional transversal sulcus (Patterson 1937). For the latter taxon, Dozo and Martínez (2015) mentioned a complex gyrification similar to that observed in the toxodontids *Adinotherium ovinum* and *Nesodon* (Radinsky 1981).

Among Typotheria, a suprasylvian sulcus and a lateral sulcus are present in the interatheriids *Miocochilius anopomodus* (Radinsky 1981), *Protypotherium* (Simpson 1933b; Dechaseaux 1962), and *Interatherium* (Radinsky 1981), but also in the hegetotheriid *Hegetotherium mirabile* (Simpson 1933b, Radinsky 1981) and most mesotheriids. Endocast linear measurements (Online Resource 3) indicate that mesotheriines (except for *M. cristatum*) and other rodent-like typotheres, such as the interatheriid *Interatherium robustum*, have laterally enlarged rostral hemispheres (FRW) in comparison with the total endocast width (CRW), in a similar way to the toxodont *Adinotherium ovinum*. Within our sample, the toxodontid *Nesodon* sp. has the relative widest temporal hemispheres. The trachytheriine *T. spegazzianus* has rostral hemispheres narrower and rostrally convergent (Fig. 1a). Comparison with Litopterna shows marked differences: in *Tetramerorhinus lucaris* (Simpson 1933b; Radinsky 1981; Forasiepi et al. 2016) and *Diadiaphorus* (Radinsky 1981), the endocast is mainly characterized by a rectangular cerebrum in dorsal view (including temporal and rostral lobes) and by the presence of a longitudinal sulcus.

Radinsky (1981) noted no similarity between the endocast of notoungulates and that of modern ungulates. According to Dozo and Martínez (2015), in living Euungulata (Perissodactyla and Artiodactyla), the forebrain flexure is not pronounced, with a poorly developed sylvian region, and an expanded neocortex bearing mostly longitudinal sulci. Orliac and Gilissen (2012) mentioned a complex gyrification pattern in early and middle Eocene North American perissodactyls, clearly distinct to the simpler pattern of coeval artiodactyls. Conversely, as observed by Radinsky (1981), the sulcal pattern of some notoungulates (e.g., *Hegetotherium mirabile* and *Protypotherium australe*) shows similarities with that of several South American caviomorph rodents (e.g., the dasyproctid *Dasyprocta azarae*, the caviid *Dolichotis patagonum*, and the chinchillid *Lagostomus maximus*). Dozo (1997) further indicated similarities between the endocast of the hegetotheriid notoungulate *Paeodotherium insigne* and the caviid rodent *Dolicavia minuscula*, especially with regard to the general shape of the braincase and sulci location and morphology. In addition to these observations, we could further found morphological similarities between typotherian (i.e., rodent-like) notoungulates and the cavioids *Hydrochoerus* and *Cavia* (Campos and Welker 1976), in terms of braincase shape and sulci location (suprasylvian and lateral sulci).

Midbrain

All the mesotheriids analyzed in this study show a dorsal exposure of the midbrain without any remarkable or varying feature.

Cerebellum

In dorsal view, the cerebellum width of *T. spegazzinianus* and of *M. maendrum* is similar to the maximum telencephalic width (FRW; Fig. 1a; Table 1; Online Resource 4); this pattern is similar in the isotemnid toxodont *Rhyphodon* sp. (Simpson 1933a). The separation between the vermis and the lateral hemisphere is well marked. The paraflocculi, housed in the subarcuate fossa of the petrosal bone (Figs. 1b, 2b, 3b and 4b; Townsend and Croft 2010; Billet and Muizon 2013) are round in shape in all studied taxa. In rostral view, the relative size of the cerebellum compared to the total endocast size is higher in *T. spegazzinianus* and *P. achirense* with respect to other endocast compared (see Table 1).

Nerves and Sinuses

In ventral view (Figs. 1c, 2c, 3c and 4c), the hypophysis region is visible in the medial plane on most of the reconstructed specimens. In *P. achirense* the orbitotemporal canal is oriented rostrodorsally in MNHN-Bol V 12664 and rostrocaudally in MNHN.F.ACH 26, whereas in all other mesotheriines studied, the orbitotemporal canal is rostrodorsally oriented, with an irregular course. The branch of the temporal vein is oriented ventrodorsally and the transverse sinus is dorsal to the latter and rostrocaudally oriented. From rostral to caudal parts, for all taxa of our sample, we have identified the following structures and foramina in the basicranium (Figs. 1c, 2c, 3c and 4c): rostral to the olfactory bulbs, the foramina of the cribriform plate through which the olfactory nerves bundles exit; the optic foramen delimiting the exit of the optic nerve (II). In the eye socket are located the exit of the orbitotemporal canal contents and the sphenorbital fissure (SOF; exit for the nerves III, IV, V_1, V_2, and VI); the piriform fenestra, which consists of a ventrally elongated foramen fused with the foramen ovale (V_3); the jugular foramen (exit for the cranial nerves IX, X, XI); and, in the caudalmost position, the hypoglossal foramen (XII) (Fig. 6).

Brain Flexure

Mesotheriid species show important differences in their endocranial morphology. In lateral view, the cerebrum-cerebellum arrangement is serial in *T. spegazzinianus* and markedly stepped in *T. alloxus* and in mesotheriine specimens. The measured telencephalic flexure angle is shallow in *T. spegazzinianus* (20.01°) whereas it is stronger in mesotheriids (24.7°-32.28°, Table 1). In our opinion, *T. spegazzinianus* retains a plesiomorphic condition for the lower telencephalic flexure and for the serial cerebrum-cerebellum arrangement, not seen in *T. alloxus* and in other mesotheriines.

Encephalization Quotient, Neocortical Ratio, and Piriform Ratio

Bodymass Estimates We made a bibliographical review of the body mass (BM) estimates for mesotheriids using regression of the length of M1, according to Croft et al. (2004) based on comparison with rodents (while the regression using extant ungulates (range 3.5–64.94 kg) seems to be underestimated in comparison with other methods used). This method provides values similar to those obtained using the multivariate craniodental algorithm 4.1 (Mendoza et al. 2006). Elissamburu (2012) indicated a range between 22.42 and 408 kg, for which the upper value is clearly overestimated and corresponds to *Trachytherus* sp. (probably *T. spegazzinianus*). In this study, we have focused mainly on the Mesotheriidae and we have decided to estimate the BM of each specimen separately (Table 2). In addition, we have recalculated and corrected the BM estimates of the taxa of the notoungulate families for which endocasts were previously studied: Interatheriidae, Notohippidae, Toxodontidae, and Hegetotheriidae (see Online Resource 2).

Encephalization Quotient Based on these EV and BM estimates for Mesotheriidae, we have calculated EQ values and obtained similar results for both *Trachytherus* species (*T. spegazzinianus* EQ1 = 0.19 and EQ2 = 0.17; and *T. alloxus* EQ1 = 0.20 and EQ2 = 0.13; Table 2; Fig. 7), *E. superans* (EQ1 = 0.23 and EQ2 = 0.22), *Typotheriopsis* "*internum*" (EQ1 = 0.28 and EQ2 = 0.26), and *M. maendrum* (MACN Pv 1111 EQ1 = 0.19 and EQ2 = 0.17; and MACN Pv 2925 EQ1 = 0.23 and EQ2 = 0.21); Table 2; Fig. 7). The highest values are found for the late Miocene *P. achirense* (MNHN.F.ACH 26 EQ1 = 0.33 and EQ2 = 0.32), while results broadly differ depending on the individual considered (MNHN Bol V 12664 EQ1 = EQ2 = 0.18; MNHN Bol V 8507 EQ1 = 0.19 and EQ2 = 0.18). The specimen documenting the latest mesotheriid of our sample, i.e., *M. cristatum* (MNHN.F.PAM 2), surprisingly has the lowest EQ values (EQ1 = 0.13 and EQ2 = 0.12) (Table 2; Fig. 7) and it also has the smallest pyriform lobes (Table 2; Fig. 5), which means that the EQ value would be increased due to a paleocortex enlargement and not to an augmentation of the neocortex.

For EQ estimates in other notoungulates, we used the BM estimate methods of Elissamburu (2012) and Cassini et al. (2012a, b) (see Online Resource 2 for complete results). For all these previously described taxa, we used the endocast volume indicated by Radinsky (1981), except for the hegetotheriid *Paedotherium insigne* for which the endocast volume value is from Dozo (1997) and the BM from Elissamburu (2004) (see Online Resource 2). We have also recalculated the EQ for the late Oligocene notohippids *Rhynchippus equinus* (EQ1 = 0.34 and EQ2 = 0.33) and *Eurygenium latirostris* (EQ1 = EQ2 = 0.26) (Online Resource 2). EQ values through time in other notoungulates, through a restricted sample, would either be invariant (in hegetotheriids; early Miocene–Pliocene) or slightly decreasing through time (in toxodontids; early Miocene–Pleistocene; Fig. 7; Online Resource 2). In addition we calculated the EQ values for the litoptern *Huayqueriana* cf. *H. cristata* (see Forasiepi et al. 2016) based on the mean of two BM methods, following Mendoza et al. (2006) and Cassini et al. (2012a, b) (EQ1 = 0.46 and EQ2 = 0.41). We have analyzed the EQ values at the ordinal level in order to compare notoungulates and Holarctic ungulates (i.e., artiodactyls; see Orliac and Gilissen 2012) for the Oligocene and Miocene epochs (Fig. 8). Boxplots highlight generally higher EQ values for the artiodactyls regardless of the studied notoungulate family and period. Such differences between both orders (artiodactyls and notoungulates) are statistically significant for Oligocene and Miocene epochs independently (Online Resource 2).

Neocorticalization Ratio Compared to the neocortical ratio (NR) of other mesotheriines with a complete endocast, *T. spegazzinianus* shows a high NR of ca. 30%, while this ratio between ca. 20–33% in other mesotheriines (Table 2). *P. achirense* (NR = 20.95% and 25.90%) shows similar values to that observed in *M. cristatum* (NR = 23.71%), and *M. maendrum* shows the highest values similar to that of *T. spegazzinianus* (NR = 32.69% and 30.06% respectively). The EQ and NR values of this latter species are unexpectedly high with respect to the rather basal phylogenetic position of this taxon (i.e., early offshoots among Mesotheriidae). Intra-mesotheriid comparison indicates NR values quite similar to those of *M. maendrum* (NR = 32.69% and 30.06%; Pliocene Montehermosan SALMA), but exceeding values measured for other taxa (with a range of NR = 23.71%–30.79%) (Fig. 5; Table 2).

Piriform ratio. The piriform ratios have highest values for *M. maendrum* (PR = 6.24% and 5.98%) and *P. achirense* (PR = 6.45% and 4.70%), followed by *T. spegazzinianus*

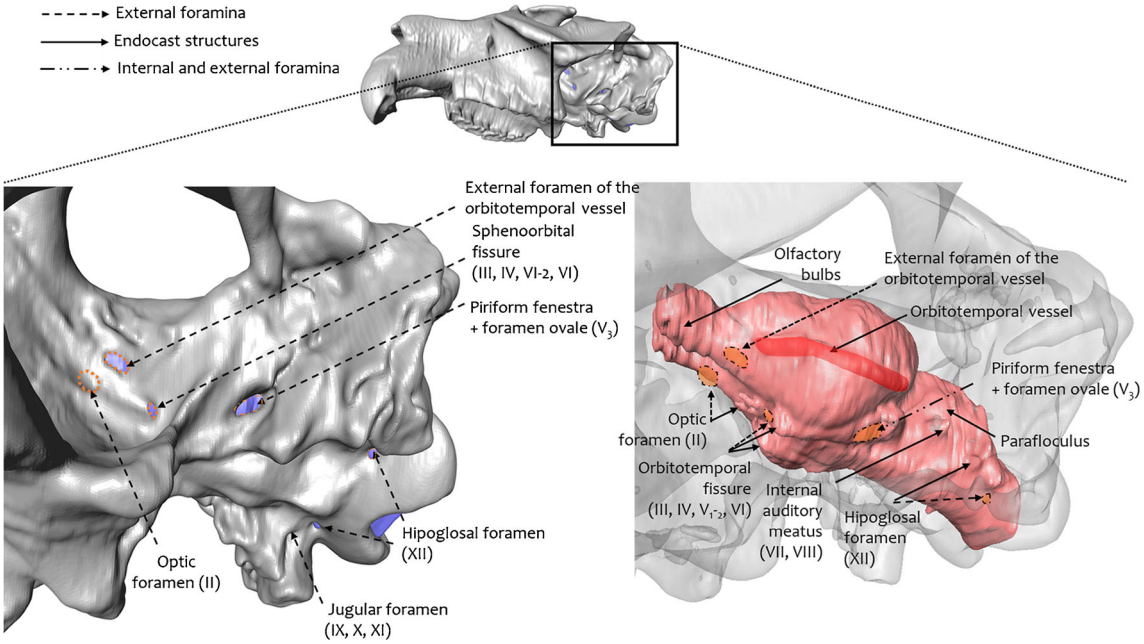

Fig. 6 Reconstruction of the caudal skull of *Mesotherium maendrum* (MACN Pv 2925) in lateroventral view

(PR = 5.03%), *E. superans* (PR = 4.75%) and finally *M. cristatum* (PR = 3.86%) (Table 2; Fig. 5).

Discussion

Evolution of Brain Size in Mesotheriids

Encephalization increase over macroevolutionary time is usually considered as a general pattern among amniotes (Jerison 1973), even if recent studies have identified some EQ modifiers, such as sociality (Shultz and Dunbar 2010) or differential locomotion (Pilleri et al. 1984). In this sense, Jerison (1973) has suggested predatory pressure as a possible driver of brain encephalization, with i) a positive selection in the case of predation by 'large-brained' predators (e.g., Holarctic ungulates being mostly preyed on by placentals) and ii) a negative or neutral selection in a context of lower predatory pressure (e.g., by 'small-brained' predators, such as marsupials, crocodylomorphs, or terror birds) or on islands, as it occurred for South American ungulates during the Cenozoic (e.g., Croft 2001). Our data, pointing to not highly variant EQs over time in Mesotheriidae, Toxodontidae, and Hegetotheriidae, would confirm this hypothesis of a neutral selective predation pressure on notoungulate brain size (Fig. 7). The sample is not sufficient regarding toxodontids to infer a temporal decrease of brain size (as depicted by EQ). In turn, we show here that mesotheriids have retained a stable brain volume over the time, most probably related to the conservative postcranial morphology in this family (Shockey et al. 2007; Shockey and Anaya 2008; Fernández-Monescillo et al. 2017). In this sense and based on evidence from rodents, Pilleri et al. (1984) had proposed that the locomotor mode acts as an EQ modifier. Bertrand and Silcox (2016) and Bertrand et al. (2016) supported this hypothesis for mammalian groups with high taxonomic and ecological diversity. This may also apply to notoungulates, the most taxonomically diversified South American ungulate clade which show a high diversity in terms of body mass and postcranial morphologies due to important niches availability and geographic isolation (Pascual et al. 1966; Alberdi et al. 1995; Bond et al. 1995). Some notoungulates are usually considered as cursorial grazing mammals (e.g., Sinclair 1909; Scott 1932; Bond 1986; Croft and Anderson 2008). Yet, recent studies focused on postcranial functional anatomy have identified mesotheriids as being semi-fossorial mammals with a scratch-digger lifestyle (e.g., Fernández-Monescillo et al. 2017). According to Pilleri et al. (1984), and based on their distinct locomotion mode, fossorial animals would show the lowest values of EQ. Among this family, the Pleistocene species *M. cristatum* shows the most derived osteological features related to accurate digging abilities (Shockey et al. 2007; Fernández-Monescillo et al. 2017). Therefore, in good agreement with what is observed in rodents, we propose here that low EQ values of mesotheriids with respect to other notoungulates (Fig. 5) would be related to their distinct semi-fossorial lifestyle. This statement would be further supported by the fact that the most fossorial of them, namely *M. cristatum*, has also the smallest EQ value at the family. The EQ values do not vary through time among mesotheriids, thus documenting a general stasis, the (with a surprising decrease for the Pleistocene *M. cristatum*) (Table 2; Fig. 7). We have identified both endocranial similarities of

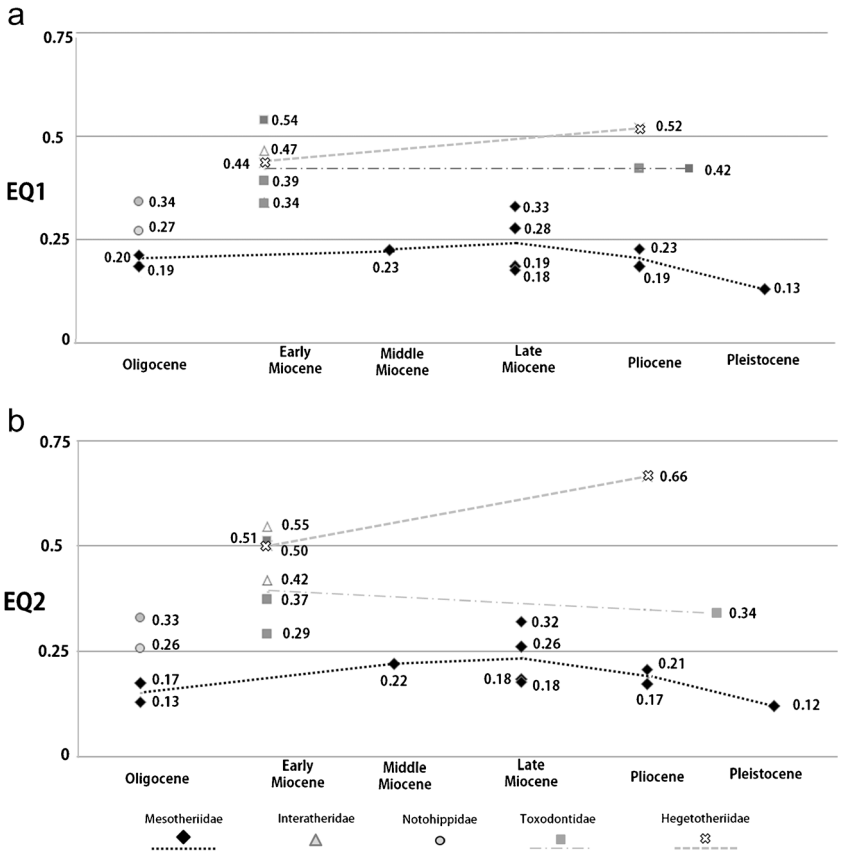

Fig. 7 **a**, Encephalization quotient estimates EQ1 (Jerison 1973) . **b,** EQ2 (Eisenberg 1981) in different notoungulate families through time (Oligocene–Pleistocene). The bodies mass (BM) used are the mean values found in the literature for each taxon (specimen in Mesotheriids). See Online Resource 2 for further details. The dashed line indicates mean values

rodent-like typotherians (e.g., mesotheriids and hegetotheriids) and some convergent morphological evolutions (e.g., high-crowned teeth, diprotodonty) with South American rodents (i.e., Chinchilloidea, Cavioidea) as a similar response to the ecological conditions that occurred in the southern part of South America since the Eocene (i.e., increasing aridity, cooling, and volcanism; Kohn et al. 2015, Gomes Rodrigues et al. 2017).

Olfaction

The piriform cortex relates to olfaction. Its size is negatively related to the size of the neocortex, and therefore directly related to the location of the rhinal fissure. In *P. achirense* (MNHN.F.ACH 26), showing the highest PR values within Mesotheriidae (ca. 6.45%), followed by *M. maendrum* (6.24% and 5.98%), the caudal part of the orbitotemporal canal (considered as the external marker for the rhinal fissure in mesotheriines) is ventrally located (Fig. 4a), and the NR is not markedly high (Table 2, Fig. 5). The piriform ratio (Fig. 5) seemingly increases from the Oligocene to the Pliocene, and *P. achirense* and *M. maendrum* would have shown the best developed olfaction among Mesotheriidae, as further indicated by the olfactory peduncles area (OPW*OPH; Table 1) and the PR values. Conversely, olfaction was probably less developed in the latest representative *M. cristatum* (late early Pleistocene) than in any other mesotheriids. We relate here the brain configuration of *M. cristatum* (e.g., increase of paleocortex and decrease of the piriform cortex) with its putative semifossorial abilities (Shockey et al. 2007, Fernández-Monescillo et al. 2017). Nevertheless, this statement is based on a single specimen and it should be investigated further in future studies. Unfortunately, no ecological or behavioral differentiation between trachytheriines and mesotheriines has been proposed thus far, likely to explain such differences. The lower values for the EQ, NR, and PR as measured in *M. cristatum* are quite surprising.

Impact of Sample Size on EQ Estimates

The EQ values of species documented by more than one specimen (e.g., *M. maendrum* and *P. achirense*) show high variations. We consider these differences as a faithful reflection of the potential intraspecific variability of a taxon (e.g., ontogenetic variation, evidenced in the sub-adult MNHN Bol V 12664). Similar EQ variations have been previously mentioned within a single subspecies of extant perissodactyls (*Equus caballus przewalskii*; see Danilo et al. 2015). The same result is observed within mesotheriids in the samples of *P. achirense* from Achiri, and of *M. maendrum* from Montehermoso. Therefore, studies on EQ based uniquely on one specimen should be taken into account cautiously.

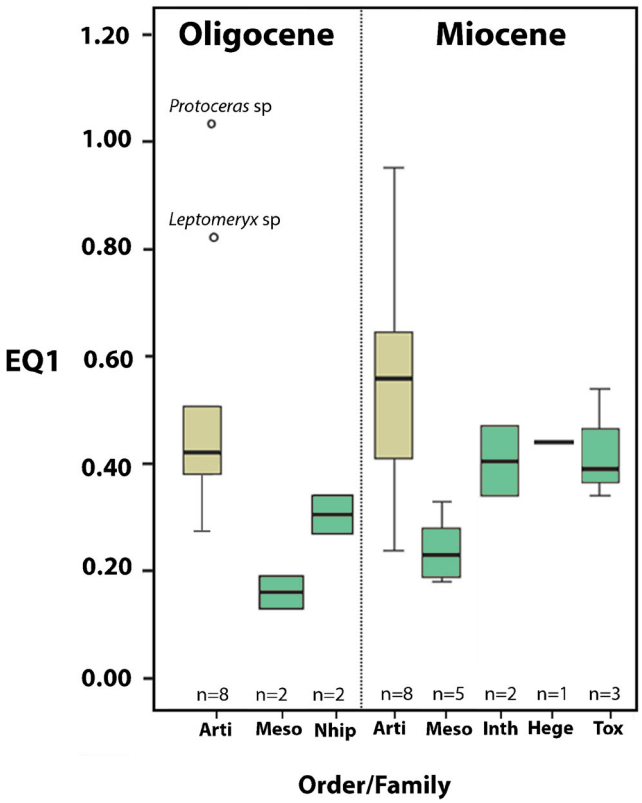

Fig. 8 Box plot of EQ1 (Jerison 1973) in Oligocene and Miocene artiodactyls and notoungulates. Data provided are included in Table 1, Online Resource 2, and Orliac and Gilissen (2012). Abbreviations: *Arti*, artiodactyl; *Hege*, Hegetotheriidae; *Inth*, Interatheriidae; *Mesot*; Mesotheriidae; *Nhip*, Notohippidae; *Tox*, Toxodontidae

Besides, bias related to intraspecific variation might exceed uncertitude related to BM estimates for EQ calculation, at least in both mesotheriid populations previously indicated (see Fig. 7 and Online Resource 2).

Conclusions

According to our morphological analysis:

1) We have identified that the orbitotemporal canal does not always correspond to the exterior mark of the rhinal fissure, and therefore does not always correspond to the neo −/paleocortex limit in notoungulates, such as *Toxodon* sp. and *Rhynchippus equinus*, or in the litoptern *Huayqueriana* cf. *H. cristata*.
2) We have described a variation for the orientation of the orbitotemporal canal among mesotheriines, either in the transverse (rostrocaudal) plane (e.g., *E. superans*, *Typotheriopsis* "*internum*", *P. achirense*), or dorsally oriented (*M. maendrum* and *M. cristatum*).
3) We have related morphological endocranial similarities between South American rodents and rodent-like typotherians (e.g., mesotheriids and hegetotheriids) to the environmental conditions having occurred in South America since the Eocene.

According to our encephalization quotient (EQ) comparisons:

1) We have inferred differential lifestyles as a positive EQ modifier between notoungulate families, with assumed semi-fossorial mesotheriids having the lowest EQ values (Fig. 7; see Pilleri 1984).
2) The relative stability of EQ among mesotheriids ('stasis') may coincide with the persistence of a scratch-digger lifestyle over time, as evidenced through postcranial morphology (Fig. 7).
3) Low predation pressure, with respect to coeval Holarctic mammalian guilds, may have allowed for retaining low brain size values in notoungulates (Fig. 8), as previously suggested by Jerison (1973), evidenced during the Oligocene and Miocene (Online Resource 2). In particular, we did not highlight any increase in the neocortical complexity for notoungulates during the Oligocene–Pleistocene interval, contrary to what was recognized for Holarctic artiodactyls, notably under higher predation pressure (Oligocene increase; Orliac and Gilissen 2012).
4) We have identified the small size of an intraspecific sample as the highly limiting factor to determine accurately the EQ of species, instead of bias inherent to BM estimates.

According to relative volume of olfactory bulbs, we infer a better developed olfactory system for the trachytheriine *T. spegazzinianus* than for *M. maendrum*. Yet, according to both piriform ratios and olfactory peduncle area, we infer the best olfaction for the Pliocene *M. maendrum* and *P. achirense* among Mesotheriidae.

The distinctive endocast morphology of *T. spegazzinianius*, as depicted by its less inflated rostral neocortex, would suggest distinct lifestyle abilities for trachytheriines and for mesotheriines.

Acknowledgments We acknowledge A. Kramarz and S. Alvarez (MACN, Buenos Aires, Argentina), C. de Muizon, C. Argot, and G. Billet (MNHN, Paris, France), and A. De Sosa Tomas (UNPSJB, Comodoro Rivadavia, Argentina) who gave access to the specimens under they care.

We kindly thank all the team members: M. A. Abello, S. Adnet, G. Billet, L. Marivaux, M. B. Prámparo, P. Münch, and R. Andrade Flores who participated in the field missions in Achiri (2010–2015). We also acknowledge staff from the UMS2700 OMSI (MNHN, Paris) for having given access to their X-ray microtomography facilities (AST-RX platform). Finally, we warmly thank S. Mosconi from the Fundación Escuela Medicina Nuclear (Mendoza, Argentina), M. Namias from the Fundación Centro Diagnóstico Nuclear (Buenos Aires, Argentina), and the personnel from MEDICENTRO clinic (La Paz, Bolivia) for providing

access to CT scanner facilities. We are grateful to the people of Achiri for facilitating our fieldwork (2010–2015). This work was notably funded by the ECOS-FonCyT program (A14U01) and the National Geographic Society (NGS 9971-16). This project was made possible thanks to the cooperation agreement between the MNHN Bol, the IANIGLA, and the ISEM (CONICET Cooperation Agreement N°864/2014). This work was also supported by the LabEx BCDiv (Laboratoire d'Excellence Biological and Cultural Diversities, http://labex-bcdiv.mnhn.fr/).

Finally, we thank Dr. John Wible, and the reviewers Dr. Darin Croft and one anonymous for their helpful and constructive comments on an earlier version of this paper.

References

Alberdi MTA, Ortiz-Jaureguizar E, Prado JL (1995) Evolución de las comunidades de mamíferos continentales del Cenozoico Superior. Rev Españ Paleontol 10: 30–36

Bertrand OC, Amador-Mughal F, Silcox MT (2016) Virtual endocasts of Eocene *Paramys* (Paramyinae): oldest endocranial record for Rodentia and early brain evolution in Euarchontoglires. Proc Roy Soy B 283: 20152316

Bertrand OC, Silcox MT (2016) First virtual endocast of a fossil rodent: *Ischyromys typus* (Ischyromyidae, Oligocene) and brain evolution in rodents. J Vertebr Paleontol 3:36

Billet G (2011) Phylogeny of the Notoungulata (Mammalia) based on cranial and dental characters. J Syst Palaeontol 9:481–497

Billet G, Muizon C de (2013) External and internal anatomy of a petrosal from the late Paleocene of Itaboraí, Brazil, referred to Notoungulata (Placentalia). J Vertebr Paleontol 33:455–469

Billet G, Muizon C de, Mamani Quispe B (2008) Late Oligocene mesotheriids (Mammalia, Notoungulata) from Salla and Lacayani (Bolivia): implications for basal mesotheriid phylogeny and distribution. Zool J Linn Soc 152: 153–200

Bond M (1986) Los ungulados fósiles de Argentina: evolución y paleoambiente. 4° Congreso argentino de Paleontología y Bioestratigrafia (Mendoza) Actas 2: 173–185

Bond M, Cerdeño E, López G (1995) Los ungulados nativos de América del Sur. In: Alberdi M T, Leone G, Tonni E P (eds) Monografías del Museo Nacional de Ciencias Naturales: CSIC, Madrid, España 12: 259–275

Brauer K, Shober W (1970) Katalog der Saugetiergehirne. In: Fischer, G (ed) Catalogue of Mammalian Brains. G. Fisher, Jena, pp 1–14

Buckley M (2015) Ancient collagen reveals evolutionary history of the endemic South American 'ungulates'. Proc Roy Soc B 282:20142671

Campos GB, Welker WI (1976) Comparisons between brains of large and a small hystricomorph rodent: capibara, *Hydrochoerus* and Guinea pig, *Cavia*; neocortical projection regions and measurement of brains subdivisions. Brain Behav Evol 13: 243–266

Cassini GH, Cerdeño E, Villafañe AL, Muñoz NA (2012b) Paleobiology of Santacrucian native ungulates (Meridiungulata: Astrapotheria, Litopterna and Notoungulata). In: Vizcaíno SF, Kay RF, Bargo S (eds) Early Miocene Paleobiology in Patagonia: High-Latitude Paleocommunities of the Santa Cruz Formation. Cambridge University Press, Cambridge, pp 243–286

Cassini GH, Vizcaíno SF, Bargo MS, Cassini G (2012a) Body mass estimate in early Miocene native South American ungulates: a predictive equation based on 3D landmarks. J Zool 287: 53–64

Cattoi N (1943) Osteografía y osteometría comparada de los géneros Typotheriodon and Typotherium. Mus Arg Cienc Nat Buenos Aires, pp 119

Cifelli RL (1985) South American ungulate evolution and extinction. In: Stehli F, Webb SD (eds) The Great American Biotic Interchange. Plenum Press, New York, pp 249–266

Cifelli RL (1993) The phylogeny of the native South American Ungulates. In: Szalay FS, Novacek MJ, McKenna MC (eds) Mammal Phylogeny, Volume 2: Placentals. Springer Verlag, New York, pp 195–216

Croft DA (1999) Placentals: endemic South American ungulates. In: Singer R (ed) The Encyclopedia of Paleontology. Fitzroy-Dearbom, Chicago, pp 890–906

Croft DA (2000) Archaeohyracidae (Mammalia: Notoungulata) from the Tinguiririca Fauna, central Chile, and the evolution and paleoecology of South American mammalian herbivores. PhD thesis, University of Chicago

Croft DA (2001) Cenozoic environmental change in South America as indicated by mammalian body size distributions (cenograms). Diversity and Distributions 7: 271–287

Croft DA (2016) Horned Armadillos and Rafting Monkeys: the Fascinating Fossil Mammals of South America. Indiana University Press, Bloomington, 320 pp

Croft DA, Anderson LC (2008) Locomotion in the extinct notoungulate *Protypotherium*. Palaeontol Electron 11:20

Croft DA, Flynn JJ, Wyss AR (2004) Notoungulata and Litopterna of the early Miocene Chucal Fauna, northern Chile. Fieldiana Geol 50: 1–52

Danilo L, Remy J, Vianey-Liaud M, Mérigeaud S, Lihoreau F (2015) Intraspecific variation of endocranial structures in extant *Equus*: a prelude to endocranial studies in fossil equoids. J Mammal Evol 22: 561–582

Dechaseaux C (1962) Encéfalos de notoungulados y de desdentados xenartros fósiles. Ameghiniana 2: 193–209

Dozo MT (1997) Paleoneurología de *Dolicavia minuscula* (Rodentia, Caviidae) y *Paedotherium insigne* (Notoungulata, Hegetotheriidae) del Plioceno de Buenos Aires, Argentina. Ameghiniana 34:427–435

Dozo MT, Martínez G (2015) First digital cranial endocasts of late Oligocene Notohippidae (Notoungulata): implications for endemic South American ungulates brain evolution. J Mammal Evol 23:1–16

Eisenberg JF (1981) The Mammalian Radiations. An Analysis of Trend in Evolution, Adaptation, and Behavior. The University of Chicago Press, Chicago and London

Elissamburu A (2004) Análisis morfométrico y morfofuncional del esqueleto apendicular de *Paedotherium* (Mammalia, Notoungulata). Ameghiniana 41: 363–380

Elissamburu A (2012) Estimación de la masa corporal en géneros del Orden Notoungulata. Estud Geol 68: 91–111

Fernández-Monescillo M, Mamani Quispe B, Pujos F, Antoine P-O (2017) Functional anatomy of the forelimb of *Plesiotypotherium achirense* (Mammalia, Notoungulata, Mesotheriidae) and evolutionary insights at the family level. J Mammal Evol pp 1–15

Forasiepi AM, MacPhee RDE, Hernández Del Pino S, Schmidt GI, Amson E, Grohé C (2016) Exceptional skull of *Huayqueriana* (Mammalia, Litopterna, Macraucheniidae) from the late Miocene of Argentina: anatomy, systematics, and paleobiological implications. Bull Am Mus Nat Hist 404: 1–76

Gomes Rodrigues H, Herrel A, Billet G (2017) Ontogenetic and life history trait changes associated with convergent ecological specializations in extinct ungulate mammals. Proc Natl Acad Sci USA 114: 1069–1074

Gervais P (1869) Mémoire sur les formes cérébrales propres aux édentés vivants et fossiles: précédé de remarques sur quelques points de la structure anatomique de ces animaux et sur leur classification. N Arch Mus hist nat Paris 74

Gervais P (1872) Mémoire sur les Formes cérébrales propres à différents groupes de mammifères. J Zool 1:425–469

Gregory WK (1910) The orders of mammals. Bull Am Mus Nat Hist 27: 1–524

Janis C (1990) Correlation of cranial and dental variables with body size in ungulates and macropodoids. In: Damuth J, MacFadden BJ (eds) Body Size in Mammalian Paleobiology: Estimation and Biological Implications. Cambridge University Press, Cambridge, pp 255–299

Jerison HJ (1973) Evolution of the Brain and Intelligence. Academic Press, New York

Jerison HJ (2012) Digitized fossil brains: neocorticalization. Biolinguistic 6:383–392

Kohn MJ, Strömberg CAE, Madden RH, Dunn RE, Evans S, Carlini AA (2015) Quasi-static Eocene–Oligocene climate in Patagonia promotes slow faunal evolution and mid-Cenozoic global cooling. Palaeogeogr Palaeoclimatol Palaeoecol 435:24–37

Kraglievich L (1930) La Formacíon Friaseana del Río Frías, etc., y su fauna de mamíferos. Physis 10:127–166

Lebrun R (2014) ISE-MeshTools, a 3D interactive fossil reconstruction freeware. Paper presented at the 12th Annual Meeting of EAVP, Torino

Lebrun R, Orliac MJ (2017) Morphomuseum: an online platform for publication and storage of virtual specimens. Paleontol Soc Pap 22:183–195

Long A, Bloch JI, Silcox MT (2015) Quantification of neocortical ratios in stem primates. Am J Phys Anthropol 157: 363–373

Loomis FB (1914) The Deseado Formation of Patagonia. Runford Press, Concord, 232 pp

Macrini TE (2009) Description of a digital cranial endocast of *Bathygenys reevesi* (Merycoidodontidae; Oreodontoidea) and implications for apomorphy-based diagnosis of isolated, natural endocasts. J Vertebr Paleontol 29: 1199–1211

Macrini TE (2006) The evolution of endocranial space in mammals and non-mammalian cynodonts. PhD dissertation, University of Texas, Austin, 278 pp

Macrini TE, Rougier GW, Rowe T (2007) Description of a cranial endocast from the fossil mammal *Vincelestes neuquenianus* (Theriiformes) and its relevance to the evolution of endocranial characters in therians. Anat Rec 290:875–892

Marshall LG, Cifelli RL (1989) Analysis of changing diversity patterns in Cenozoic land mammal age faunas, South America. Palaeovertebrata 19: 169–210

McKenna MC (1975) Toward a phylogenetic classification of the Mammalia. In: Luckett WP, Szalay FS (eds) Phylogeny of the Primates: A Multidisciplinary Approach. Plenum Press, New York, pp 21–46

McKenna MC, Bell SK (1997) Classification of Mammals Above the Species Level. Columbia University Press, New York, 631 pp

Mendoza M, Janis CM, Palmqvist P (2006) Estimating the body mass of the extinct ungulates: a study on the use of multiple regression. J Zool 270: 90–101

Oiso Y (1991) New land mammal locality of the middle Miocene (Colluncuran) age from Nazareno, southern Bolivia. In: Suarez-Soruco R (ed) Fósiles y Facies de Bolivia, Vertebrados Yacimientos Petrolíferos Fiscales Bolivianos. Santa Cruz, Bolivia, pp 653–672

Orliac MJ, Gilissen E (2012) Virtual endocranial cast of earliest Eocene *Diacodexis* (Artiodactyla, Mammalia) and morphological diversity of early artiodactyl brains. Proc Roy Soc B 279 (1743):3670–3677

Pascual R, Ortega-Hinojosa EJ, Gondar D, Tonni EP (1966) Paleontografía bonaerense (Vol. 6). La Plata: Anales de la Comisión de Investigación de Buenos Aires, La Plata, 202 pp

Patterson B (1934) *Trachytherus*, a typotherid from the Deseado beds of Patagonia. Geol Ser Field Mus Nat Hist 6:119–139

Patterson B (1937) Some notoungulate braincasts. Geol Ser Field Mus Nat Hist 6:273–301

Patterson B, Pascual R (1968) The fossil mammal fauna of South America. Q Rev Biol 43:409–451

Pilleri G, Gihr M, Kraus C (1984) Cephalization in rodents with particular reference to the Canadian beaver (*Castor canadensis*). In: Pilleri G (ed) Investigations on Beavers. Brain Anatomy Institute, University of Berne, pp 11–102

Radinsky L (1978) Evolution of brain size in carnivores and ungulates. Am Nat 112: 815–831

Radinsky L (1981) Brain evolution in extinct South American ungulates. Brain Behav Evol 18:169–187

Radinsky LB (1984) Ontogeny and phylogeny in horse skull evolution. Evolution 38: 1–15

Reguero MA, Prevosti FJ (2010) Rodent-like notoungulates (Typotheria) from Gran Barranca, Chubut Province, Argentina: phylogeny and systematics. In: Madden RH, Carlini AA, Vucetich MG, Kay RF (eds) The Paleontology of Gran Barranca: Evolution and Environmental Change through the Middle Cenozoic of Patagonia. Cambridge University Press, Cambridge, pp 148–156

Rovereto C (1914) Los estratos araucanos y sus fósiles. Anales Mus Nac Hist Nat Buenos Aires 25:1–250

Rowe T (1996) Coevolution of the mammalian middle ear and neocortex. Science 273: 651–654

Scott KM (1990) Postcranial dimensions of ungulates as predictors of body mass. In: Damuth J, MacFadden BJ (eds) Body Size in Mammalian Paleobiology: Estimations and Biological Implication Cambridge University Press, Cambridge, pp 301–335

Scott WB (1932) Nature and origin of the Santa Cruz fauna with additional notes on the Entelonychia and Astropotheria. Reports of the Princeton Expeditions to Patagonia 1896–1899 vol 7:157–192

Serres M (1867) De l'ostéographie du *Mesotherium* et de ses affinités zoologiques. C R hebd Acad Sci 65:140–148

Shockey BJ, Anaya F (2008) Postcranial osteology of mammals from Salla, Bolivia (late Oligocene): form, function, and phylogenetic implications. In: Sargis EJ, Dagosto M (eds) Mammalian Evolutionary Morphology: A Tribute to Frederick S. Szalay. Springer Netherlands, Dordrecht, pp 135–157

Shockey BJ, Croft DA, Anaya F (2007) Analysis of function in the absence of extant functional homologues: a case study using mesotheriid notoungulates (Mammalia). Paleobiology, 33: 227–247

Shultz S, Dunbar R (2010) Encephalization is not a universal macroevolutionary phenomenon in mammals but is associated with sociality. Proc Natl Acad Sci USA 107: 21582–21586

Silcox MT, Dalmyn CK, Hrenchuk A, Bloch JI, Boyer, DM, Houde P (2011) Endocranial morphology of *Labidolemur kayi* (Apatemyidae, Apatotheria) and its relevance to the study of brain evolution in Euarchontoglires. J Vertebr Paleontol 31: 1314–1325

Simpson GG (1932) Skulls and brains of some mammals from the *Notostylops* beds of Patagonia. Am Mus Novitates 578:1–11

Simpson GG (1933a) Braincast of *Phenacodus*, *Notostylops* and *Rhyphodon*. Am Mus Novitates 622:1–19

Simpson GG (1933b) Braincasts of two typotheres and a litoptern. Am Mus Novitates 629:1–18

Simpson GG (1948) The beginning of the age of mammals in South America. Part 1. Systematics: Marsupialia, Edentata, Condylarthra, Litopterna and Notioprogonia, Bull Am Mus Nat Hist 91:1–232

Sinclair WJ (1909) Mammalia of the Santa Cruz beds. Part I. Typotheria. Reports of the Princeton Expeditions to Patagonia 1896–1899, vol 6:1–110

Stirton RA (1953) A new genus of interatheres from the Miocene of Colombia. Calif Univ Dept Geol Sci B 29(6):265–347

Townsend B, Croft DA (2010) Middle Miocene Mesotheriine diversity at Cerdas, Bolivia and a reconsideration of *Plesiotypotherium minus*. Palaeontol Electron 13:36

Welker F, Collins MJ, Thomas JA, Wadsley M, Brace S, Cappellini E, Turvey ST, Reguero M, Gelfo J, Kramarz A, Burger J, Thomas-Oates J, Ashford DA, Ashton PD, Porter DM, Kressler B, Fischer R, Baessmann C, Kaspar S, Olsen JV, Killey P, Elliott JA, Christian DK, Mullin V, Hofreiter M, Willerslev E, Hublin J-J, Orlando L, Barnes I, MacPhee RDE (2015) Ancient proteins resolve the evolutionary history of Darwin's South American ungulates. Nature 522: 81–84